Rydberg molecule in a magnetic field

N. Shafizadeh, M. Raoult, M. Horani, S. Guizard, D. Gauyacq

Classification
Physics Abstracts
33.35 — 33.45B — 33.80

Rydberg molecule in a magnetic field

N. Shafizadeh, M. Raoult, M. Horani, S. Guizard and D. Gauyacq

Laboratoire de Photophysique Moléculaire du CNRS, Bât. 213, Université de Paris-Sud, 91405 Orsay Cedex, France

(*Received 6 December 1991, accepted 21 January 1992*)

Abstract. — Rydberg states of the NO molecule have been probed by two-color resonantly enhanced multiphoton ionization in a magnetic field of 0.93 T. Penetrating s and d states show strong interactions with the intramolecular field while nonpenetrating f states show stronger interactions with the external magnetic field. Competition between the molecular core anisotropy and the external field anisotropy leads to a greater variety of situations than in a Rydberg atom, ranging from a « weak field » regime to a « strong field » regime. These different situations are illustrated by a multichannel quantum defect calculation on the np states of NO including the Zeeman effect. An extreme situation can be achieved in which the Rydberg molecule looses its molecular character and shows an almost pure atomic structure within each rotational channel.

1. Introduction.

A Rydberg molecule consists of a molecular core positively charged and an electron in a highly excited orbital corresponding to a high principal quantum number in the united atom limit. In addition to the dominant Coulomb attraction from the core, the Rydberg electron experiences the molecular anisotropy during the short time it spends in the core region. Complicated interactions occurring at short distances (short range interactions) mostly affect the structure of the Rydberg states with low ℓ values ($\ell \leq 2$), corresponding to a penetrating Rydberg orbital. Nonpenetrating Rydberg states also experience the anisotropy of the molecular core *via* long range interactions, mainly due to the quadrupole moment and polarizability of the core which never vanish even at very large distances from the core [1]. All these interactions can be taken into account by a quantum defect parameter $\mu_{\ell\lambda}$ depending both on the angular momentum ℓ of the electron and on its projection λ on the molecular axis. As in Rydberg atoms, large quantum defects $\mu_{\ell\lambda}$ characterize penetrating states while small (near zero) $\mu_{\ell\lambda}$ values characterize nonpenetrating states (f, g, ...). In addition, the stronger the molecular anisotropy, the larger the difference between the $\mu_{\ell\lambda}$ values for different λ's and same ℓ.

This discussion will be restricted to diatomic species for simplicity. In this respect, the NO molecule is a model system for one-electron Rydberg molecules since the ground state of the ion NO^+ has a closed-shell $^1\Sigma^+$ symmetry [2]. Therefore, all the electronic properties of the Rydberg states of NO will directly depend on the character of the Rydberg orbital $\ell\lambda$. In particular, all the Rydberg states of NO converging to the ground state of NO^+ are

doublet states with $s = S$ and $\lambda = \Lambda$, where s and λ are the spin and the projection of the orbital angular momentum of the Rydberg electron, respectively, and S and Λ are the electronic spin and the projection of the orbital total angular momenta of the Rydberg state, respectively.

In addition to the molecular anisotropy, another important effect occurs in Rydberg molecules, i.e., the coupling of the Rydberg electron with the vibrational and rotational motions of the core. Vibrational coupling arises from the dependence of the quantum defect with internuclear distance or, in other words, from the difference between the Rydberg state and the ion core potential energy curves. Although this vibrational coupling can be very important and responsible for autoionization processes, it will be disregarded in this paper. The rotational coupling arises from the off-diagonal term $BJ^+ L^-$ of the rotational Hamiltonian of the molecule (B is the rotational constant, J and L are the total angular momentum and the electronic orbital angular momentum respectively) which couples nearby Λ and $\Lambda \pm 1$ electronic components within a given $n\ell$ Rydberg complex [1]. Such a rotational coupling in molecular Rydberg states is called ℓ *uncoupling* because its trend is to decouple ℓ from the internuclear axis and to couple it to the rotational axis defined by the total angular momentum minus spin of the ionic core, N^+. This ℓ uncoupling increases when the splitting between the Λ components decreases and when the rotation of the core increases (large N^+). In the limit of a very large ℓ uncoupling, the so-called Hund's case (d), Λ is no longer a good quantum number and the Rydberg states are better described by N^+ as it will be discussed below.

The aim of the present work is to study the effects of an external magnetic field on such a Rydberg molecule and the competition between the external field perturbation and the intramolecular field perturbation on the Rydberg electron. The effects of the magnetic perturbation by a moderately strong field of about 1 T will be studied both for penetrating (6s, d) and non penetrating states (4f, 15f) excited by double resonance multiphoton excitation. An MQDT approach including the linear Zeeman perturbation will also be described on the example of the penetrating np series, in order to stress out the role of the molecular anisotropy.

2. The double resonance multiphoton ionization technique.

In the energy region of high Rydberg states near the first ionization potential, the density of molecular states is very high because of the overlap of not only Rydberg series converging to this ionization limit but also other excited electronic states (Rydberg or valence states), including their vibrational and rotational structures. In addition, such an energy region usually lies above the first dissociation limit, so that continuum states overlap the numerous discrete states as well.

The spectral congestion in this region can be greatly reduced by using a highly selective excitation process. Such a selectivity is achieved by combining the double resonance technique with the multiphoton excitation process, as it has been extensively used on the studies of the NO Rydberg states in the last past years [3-12]. The first laser pumps a given electronic, vibrational, rotational intermediate level. From this intermediate level, only a very small number of excited levels are probed with the second laser. Once these Rydberg levels are excited they can be detected by ionization. The ionization step can proceed through field ionization, or photoionization with a further photon, or *via* autoionization when the levels of interest lie above the first ionization limit.

Figure 1 shows the excitation process which has been used to observe the 6s and 6d ($v = 0$) Rydberg states of NO from the intermediate $C\,^2\Pi$, $3p\pi$ ($v = 0$) state. The experimental set-up has been described elsewhere [13]. Briefly, it consists of an ionization

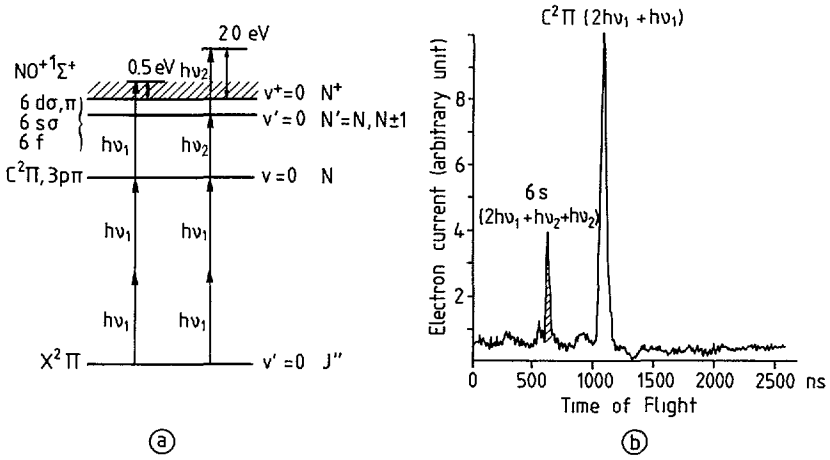

Fig. 1. — a) Excitation scheme of the 6s, 6d, 6f, $v' = 0$ Rydberg states by using two-color resonant multiphoton ionization *via* the intermediate C $^2\Pi$, 3 pπ, $v = 0$ state. b) Photoelectron time-of-flight spectrum corresponding to the excitation processes shown in (a). The slow electron peak around 1 100 ns corresponds to an electron kinetic energy of 0.5 eV, i.e. to the one-color, two-photon resonant, three-photon ionization *via* the C state at 382.6 nm (Q_{12}(9 1/2) line of the C ← X transition). The fast electron peak at 640 ns corresponds to an electron kinetic energy of 2.0 eV related to the two-color, four-photon ionization process *via* the 6s state (the probe laser was set on the Q(10) line of the 6s ← C transition at 522.8 nm). The nearby small photoelectron around 550 ns corresponds to the same two-color resonant excitation process of the 6s state except that the ionization photon comes from the pump laser at 382.6 nm (this last process is not shown in (a)).

chamber equipped with a « magnetic bottle » photoelectron time-of-flight spectrometer [14]. The two counter propagating laser beams (pump and probe) are focused with two 15 cm focal length lenses in the high field region of the magnetic bottle (field strength of 0.93 T). The two laser intensities have been kept as low as possible in order to avoid saturation and broadening effects. Typical pulse energies were of the order of 100 μJ for the pump laser and 30 μJ for the probe laser.

The double resonance spectra of the 6s, 6d states and of the 4f state were recorded at « low resolution », i.e. with a probe laser bandwidth of 0.3 cm^{-1} In the experiment corresponding to the diagram of figure 1a, no time delay was introduced between the pump and the probe laser because of the short lifetime of the intermediate C ($v = 0$) state (a few ns) [11].

A time-of-flight (TOF) analysis was first performed in order to characterize the ionization process involved in the experiment. A typical TOF spectrum is shown in figure 1b, with the two laser wavelength fixed at a two-photon pump transition and a one-photon probe transition, respectively. Then, the double resonance MPI spectrum was recorded as a function of the probe laser wavelength by collecting the total time averaged electron current. In the particular example of figure 1, one can see one advantage for using such a spectrometer. Indeed, the one color (2 + 1) three photon ionization process *via* the C state is in all cases much stronger than the two color (2 + 1 + 1) ionization *via* the 6s, d states. Both resonant states C $^2\Pi$, 3pπ ($v = 0$) and 6s ($v = 0$) have a comparable photoionization cross section. The direct photoionization process is therefore more efficient than the two step ionization process *via* the 6s state and it is even more favored due to the lower energy gap above threshold than in the two step process. This means that the double resonance ionization signal is expected to be overlapped by a stronger ionization continuum signal originating from the

three-photon ionization of the intermediate C state when the probe laser is scanned. This drawback was easily overcome by setting a retarding voltage of 0.6 V in the spectrometer which completely moved away the electron signal due to pump laser only.

In the experiments concerning the nf ($v = 1$) states, the intermediate Rydberg state $A\,^2\Sigma^+$, $3s\sigma$ ($v = 1$) was pumped *via* a two-photon transition since it was previously shown that the small d character of the Rydberg orbital of the A state leads to significant oscillator strength of the nf states [4].

Among all excited states energetically accessible in these two color MPI experiments, only a few Rydberg states can be observed. They will be those allowed by the electronic quasi-atomic selection rules, i.e. np states and nf states from the intermediate A state and ns, nd states from the intermediate C state. In addition, Franck-Condon factors strongly favor the observation of $\Delta v = 0$ Rydberg-Rydberg transitions as indicated in figure 1a. From one rotational intermediate level N, only three rotational upper levels of a given electronic component can be populated *via* R, Q and P transition lines (with $\Delta N = +1, 0$ and -1, respectively).

In the experiments presented here, the ionization step either is saturated or varies very slowly with probe photon energy [11]. Under these conditions, the detected ion signal only reflects the Rydberg-Rydberg transition intensities when the probe laser wavelength is scanned. It gives direct information on the structure and, eventually, on the relaxation of the high Rydberg states.

3. Intramolecular field effects in a Rydberg molecule.

In this section, we will briefly describe the rotational-electronic structure of molecular Rydberg states in the absence of any external field. Indeed, the degree of decoupling of the angular momentum ℓ of the Rydberg electron from the molecular frame governs the efficiency of the magnetic perturbation on this electron as we will discuss in the next section.

In addition to the dominating Coulomb attraction, the Rydberg electron can experience two types of coupling with the molecular core.

The first coupling is an electrostatic coupling induced by the anisotropy of the molecular core. As said above, it leads to a lift of degeneracy of the ℓ levels into λ components. Figure 2 illustrates the effect of this anisotropy on the Rydberg complexes of NO, following a diagram proposed earlier by Miescher [15] and built from both absorption data [2] and MPI data [7, 10-12]. For all Rydberg states, the effect of the molecular field decreases rapidly with n, roughly as $1/n^3$, as the Rydberg electron moves farther and farther from the molecular core. As a consequence, one can define an effective anisotropy which depends not only on ℓ, i.e. on the penetrating character of the Rydberg orbital, but also on the principal quantum number n, with the corresponding scaling law in $1/n^3$.

This figure also shows how the $(n + 1)$ s, nd and nf states come closer to each other with increasing n in such a way that they form a bunch of close lying levels which are called « n supercomplexes » as earlier proposed by Miescher [15] (they include not only different λ components but also different ℓ components). As pointed out by Miescher, these different components of the same supercomplex may interact (for instance by ℓ uncoupling and/or ℓ mixing) or they may not interact at all. In particular, the s and d states are strongly mixed (mixing coefficients of almost 50 %) in NO [16, 11]. These s and d states experience penetration effects of different origins depending on the λ component, as described in details by Jungen [16]. As a consequence, the $d\delta$ component lies quite far below the other two components of the d complex (with a quantum defect of about $+0.08$) while the $d\sigma$ and $d\pi$ components overlap each other (quantum defect of about -0.05) and experience

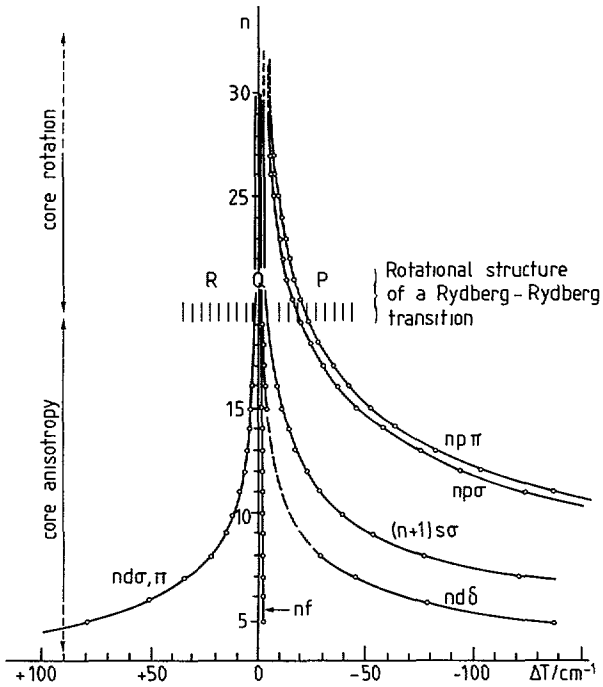

Fig. 2. — Energy diagram of the NO complexes : the principal quantum number n is plotted against the vertical axis while, on the horizontal axis, ΔT shows the difference between the observed electronic term values and the Rydberg formula (zero quantum defect). Rydberg states with positive quantum defect are plotted on the right side of the diagram (negative ΔT) while Rydberg states with negative quantum defect are plotted on the left side of the diagram (positive ΔT). Observed term values have been taken from absorption data [1] and from REMPI data [2-6].

both large ℓ uncoupling ($d\Pi^+ - d\Sigma^+$) and ℓ mixing ($d\Sigma^+ - s\Sigma^+$) [11, 12, 16]. On the other hand, as shown in figure 2, the np complexes form an isolated Rydberg series with a quantum defect of about 0.5 indicating a strong effective molecular anisotropy [2, 7].

The second type of coupling, the ℓ uncoupling, occurs between the Rydberg electron and the rotation of the molecular core. For high n Rydberg states, the orbital motion of the electron becomes slower than the rotation of the nuclei and a breakdown of the Born-Oppenheimer gradually takes place when n increases. This situation occurs when the rotational energy spacings become of the same order of magnitude or larger than the electronic spacings within a given supercomplex. This rotational spacings are mainly governed by the rotation of the molecular core, and therefore, do not change with n. As an example a typical rotational structure corresponding to a Rydberg-Rydberg transition is displayed in figure 2. In the limiting situation where the core rotation is much faster than the orbital motion of the Rydberg electron (Hund's case (d)), ℓ does not quantize any more on the internuclear axis but rather on the rotational axis of the rotating core defined by the vector $\mathbf{N}^+$, with the projection $\mathfrak{L} = N - N^+$ (the coupling scheme is given by $\mathbf{N} = \mathbf{N}^+ + \mathbf{l}$) [1]. The structure is then dominated by the rotational structure of the core and the electronic structure due to the core anisotropy appears as a small substructure for each N^+ level, defined by $\mathfrak{L}$ or N. For the nonpenetrating nf states this decoupled situation occurs already for the lowest members of the nf series (4f, 5f, .), while, for the penetrating np states two different ranges

of n can be roughly distinguished as indicated in figure 2 : the low n levels for which the molecular anisotropy is the dominating interaction leading to a Born-Oppenheimer situation with well defined Λ electronic components, and the high n levels for which the rotation of the core dominates the structure.

For the nonpenetrating nf states of the NO molecule, the core anisotropy reduces to long range interactions due to the quadrupole and the polarizability of the molecular core as was described in detail by Jungen and Miescher [1]. This long range interaction can be calculated analytically [1, 17, 13] and leads to the lift of degeneracy of the ℓ or N electronic components of the same rotational level N^+, as shown in figure 3a for the 4f and for the 15f levels. The only difference between the electronic ℓ splittings of the 4f and the 15f levels is indicated on their respective energy scales and reflects the $1/n^3$ scaling law for the long range interaction on these nf states. Note that, in this Hund's case (d) situation, the quantum number N ($N = \ell + N^+$) is related to an electronic fine structure rather than to a rotational structure as it would be the case in a Born-Oppenheimer situation (Hund's case (b)). The rotational structure is in turn described by the quantum number N^+ of the rotating core. As pointed out by Jungen and Miescher [1], the 4f level still experiences small penetration effects which lead to small deviations of the observed rotational structure compared to the calculated structure from the pure long range interactions. Figure 3b shows the observed energy diagram for the molecular anisotropy of the 4f, $v = 1$ level [4] for comparison. It can be seen that, except for the lowest rotational levels (for which Hund's case (d) is not yet achieved), the agreement is good between the calculated (Fig. 3a) and the observed (Fig. 3b) structures.

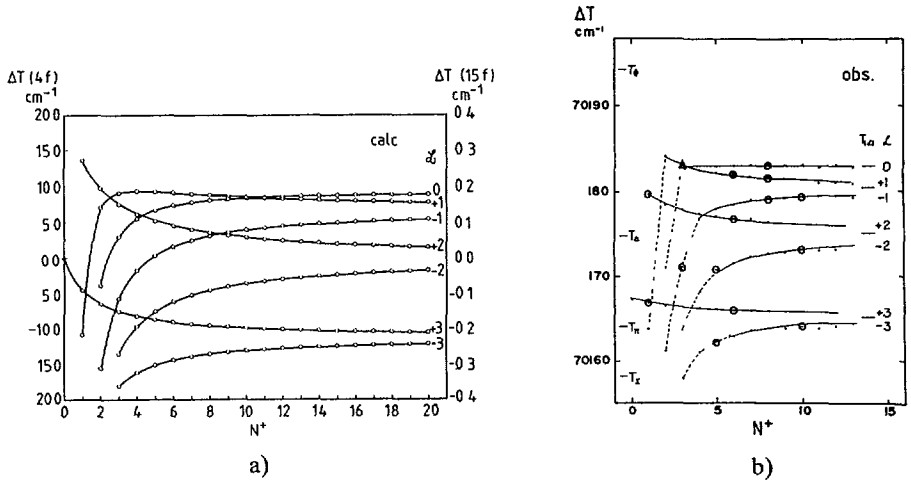

Fig. 3. — a) Calculated electronic energy splittings of the nf sublevels due to the molecular anisotropy (long range interactions in this case) and plotted against the rotational quantum number N^+ of the NO^+ core. ΔT is given by $\Delta T = T - T_0(nf) - B^+ N^+ (N^+ + 1)$ where T is the total electronic-rotational term value, $T_0(nf)$ is the rotationless term value excluding the anisotropic contributions, and $B^+ N^+ (N^+ + 1)$ is the rotational energy of the molecular core. Note the difference between the energy scales for the 4f (on the left) and for the 15f (on the right), due to the $1/n^3$ scaling law for the long range interaction (see the text). This figure is similar to the figure of reference [13] except that the scale on the left side corresponds now to the 4f state and the scale on the right side (15f state) is wrong in reference [13] and has to be replaced by the above scale [Note of the authors]. b) Observed energy splittings of the 4f level taken from reference [4]. Circle marks correspond to the observed levels of figure 7, the triangle mark corresponds to zero-field accidental degeneracy between the $N^+ = 3$, $\ell = 0$ ($N = 3$) and $N^+ = 3$, $\ell = 1$ ($N = 4$) levels (see the text).

4. Rydberg molecules in an external magnetic field.

In a *Rydberg atom,* a strong field situation occurs when the magnetic perturbation dominates the Coulomb structure. In a *Rydberg molecule,* the presence of an intrinsic fine structure, as described in section 2 above, gives rise to a larger variety of field regimes. These different regimes are related to the competition between the anisotropy induced by the external field and the intramolecular anisotropy on the one hand, and the competition between the anisotropy of the external field and the coupling to the core rotation on the other hand. Another complication arises from the fact that these different interactions act in two different frameworks : the molecular anisotropy effects are well described in the molecular frame while the field anisotropy is better described in the laboratory frame. The magnetic perturbation operator for a one electron system can be written as follows :

$$W_{\text{magn}} = \mu_B (L_z + 2\,S_z) \cdot B + \frac{e^2}{8\,m} B^2 r^2 \sin^2\theta \qquad (1)$$

where μ_B is the Bohr magneton, B is the field strength, e and m are the charge and the mass of the electron, respectively, and r and θ are the polar coordinates of the electron. The Z axis of the laboratory frame is chosen along the field axis. L_z and S_z are the electronic orbital and spin angular momenta along Z, respectively. In the experiments described here the field strength was constant and equal to 0.93 T.

The first term of equation (1) is responsible for the linear Zeeman effect (LZE). In a 1 T field this perturbation is roughly of the order of $\mu_B B \simeq 0.5\ \text{cm}^{-1}$ The second term represents the quadratic Zeeman effect (QZE). For a Rydberg species it is proportional to $n^4 B^2$. In a 1 T field, this perturbation is negligible for the low lying Rydberg states. It becomes comparable to the linear Zeeman term for $n \geqslant 35$. For even higher n values it increases rapidly and soon becomes the dominant perturbation in the molecular system. In this work we will restrict the discussion to Rydberg states with $n \leqslant 22$. Therefore, we will only consider the linear term (LZE) of the magnetic perturbation.

4.1 THE LINEAR ZEEMAN EFFECT IN THE 6s, d, 4f AND 15f STATES OF NO. — One important effect of the field anisotropy is to mix different N levels with $\Delta N = 0, \pm 1$ [18, 13]. Only the total parity and the projection M_N of N along the field axis remain good quantum numbers. The resulting structure mainly depends on the relative strength of the magnetic perturbation compared to the intramolecular couplings. The following examples on the 6s, d states and on the 4f and 15f states will illustrate situations for which the linear Zeeman effect varies gradually from a small perturbation to a strong perturbation.

In the absence of any field, the 6s, d states exhibit a strong effective molecular anisotropy, leading to a Born-Oppenheimer structure with well defined λ electronic components except for the $'d'\ \sigma\ ^2\Sigma^+$ and $'d'\ \pi\ ^2\Pi^+$ components which are strongly mixed by ℓ uncoupling. In addition, strong s-d mixing affects the Σ^+ components in such a way that the $'d'\ \Sigma^+$ and $'s'\ \Sigma^+$ levels do not have a pure $\ell = 2$ and $\ell = 0$ character, respectively. The transition diagram for this 6s, d supercomplex from a rotational level of the intermediate $C\ ^2\Pi$ state is schematically shown in figure 4. On the left side of this figure, the upper levels mainly conform to Hund's case (b) and correspond to the observed structure. The middle part of the diagram corresponds to the case (d) limit for a pure d complex with the main structure governed by the rotation of the core and described by the good quantum number N^+ and applies for high nd complexes. On the right side of this diagram, the case (b) and case (d) are equivalent to describe the ns states since $N' = N^+$ for $\ell = 0$. Note that in this figure as well as in the rest of this paper (except for Fig. 2) we have adopted the same label n for the

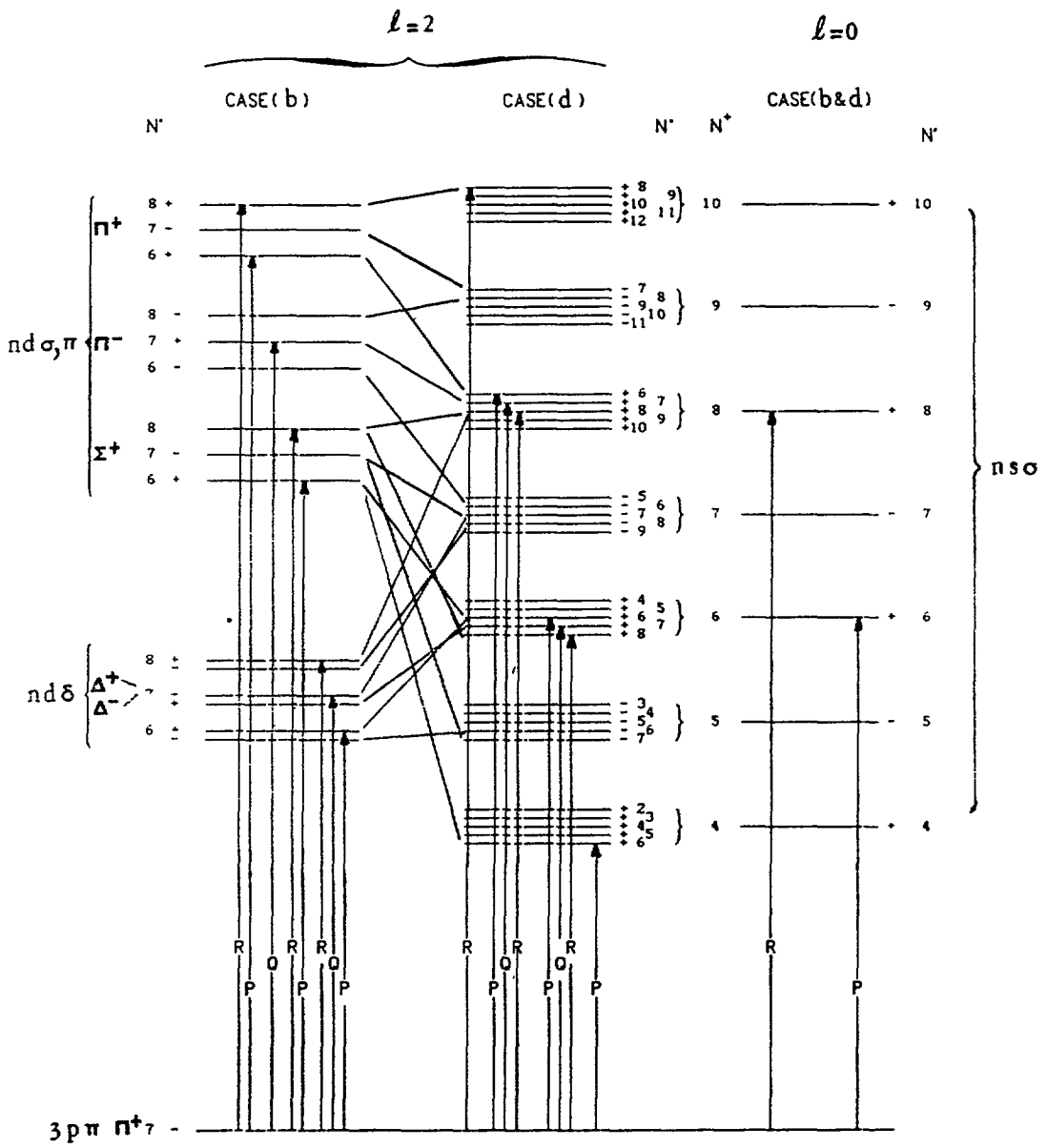

Fig. 4. — Transition diagram for the *n*s, *n*d ($v = 0, N'$) ← C $^2\Pi(v = 0, N = 7, \Pi^-)$ probe step of the two-color REMPI process. In the zero field experiment (see Fig. 5d), the intermediate rotational level $N = 7$ (Π^+ symmetry) of the C state is pumped by the two-photon $N_{12}(9\ 1/2)$ line. On the left : allowed transitions to the *n*d complex in Hund's case (b) representation, holding for low *n* principal quantum numbers. The close lying *n* dσ, π components exhibit strong ℓ-uncoupling resulting into a strong mixing between the dΣ^+ and dΠ^+ components (see the text). The dδ component, located at a lower energy, exhibit a pure case (b) character with a Λ doubling $\Delta^+ - \Delta^-$ smaller than the rotational spacing. On the middle : allowed transitions in the case (d) limit, holding for very high *n*d states and showing 8 allowed series converging to $N^+ = 4$, 6, 8 and 10. On the right : allowed transitions to the *n*s, Σ^+ component in both case (b) and case (d). The small spin splitting of each level is not shown in this diagram, for simplicity.

supercomplexes of NO as in references [11, 12], that is n differ by -1 from earlier values for the s states [2]. The correlations between case (b) and case (d) levels for the $\ell = 2$ are only approximate and indicate the main contributions of the case (d) N', N^+ levels within each N', Λ level of the 6d complex [11].

Five transitions are expected to the 6dσ, π component among which only two, i.e., P(Π^+) and R(Σ^+), have a significant intensity according to a zero field earlier multichannel quantum defect (MQDT) analysis [11]. Three transitions are allowed to the dδ component (P, Q and R) and two transitions are allowed to the sσ component (R and P). In the high n limit one expects then to observe transitions belonging mainly to two rotational channels, $N^+ = 6$ and $N^+ = 8$. For intermediate levels with Π^- symmetry and total positive parity, the allowed transitions correspond to the opposite parity in the upper levels. In this case, only odd N^+ (5, 7 and 9) are populated and the sσ component is excited *via* a Q line only.

Figure 5 shows one part of the corresponding double resonance spectrum for various intermediate rotational and parity levels within a 0.93 T magnetic field. Only the lower energy part of the 6s, d supercomplex corresponding to the dδ and sσ component is displayed in this figure. The Zeeman effect in the C $^2\Pi \leftarrow$ X $^2\Pi$ two photon transition has been analysed in a previous work [19]. Briefly the Zeeman structure of this transition consists of spin doublets $M_s = \pm 1/2$ due to a Paschen-Back effect for the spin in the upper C state and separated by $2\,\mu_B B$ ($\simeq 1$ cm^{-1}). The upper state quantum numbers N' and parity $\Pi^\pm$ are conserved. The same Paschen-Back structure for the spin is expected for the upper 6s, d complex but it cannot be observed in the probe step because of the $\Delta M_{s=0}$ selection rule for the Rydberg-Rydberg transitions. The resulting double resonance spectrum shows a pattern very similar to the zero field spectrum as shown by the similarity between the spectra of figures 5c and 5d. Note that the spectra of figures 5b and 5c are superpositions of two double resonance spectra due to partial overlap between the corresponding two-photon pump lines. Figure 5b is mainly probed from the intermediate level $N = 10$, Π^- and, to a less extend, from the $N = 7$, Π^+ intermediate level. The spectrum of figure 5c is mainly probed from the $N = 7$, Π^+ intermediate level and, to a less extend, from the $N = 7$, Π^- intermediate level, as shown by the relative R and Q line intensities in the sσ component.

In these levels, the magnetic field perturbation is very weak and does not significantly change the zero-field energy level pattern (except for the M_s splitting) as can be seen by comparing the 1 T field spectrum of figure 5c and the zero field spectrum of figure 5d. The M'_N Zeeman splitting within each N' level is smaller or of the same order of magnitude as the experimental resolution. The only observable difference concerns the 6f levels which are observed *via* local perturbation with the 6d levels. These f levels obviously exhibit a Zeeman broadening larger than the experimental bandwidth. In order to observe the Zeeman effect in this 6s, d complex a resolution 10 times better should be used.

On the other hand, zero field transitions to the nonpenetrating nf states follow the case (b)-to-case (d) selection rules as shown in the diagram of figure 6. In this case the intermediate state is the $N = 8$ rotational level of the A $^2\Sigma^+$ state. Three distinct groups of lines are allowed, belonging to three rotational channels, $N^+ = 6$, 8 and 10. Among all the N' sublevels of each N^+ value only three of them are observable *via* the selection rules $\Delta N = +1$, 0 and -1. The N' ordering within each N^+ corresponds to the long range interaction splittings shown in figure 3. Note that the R, Q and P transitions are no longer related to the upper state rotational structure as they were in the case of the 6s, d levels (see above) but rather to an electronic fine structure due to the molecular anisotropy. The splitting between these three lines is in this case a direct measure of the anisotropic interaction experienced by the Rydberg electron.

Figure 7 shows the corresponding double resonance spectra from the $N = 8$ and $N = 3$ levels of the intermediate A state, without and with an external magnetic field. For

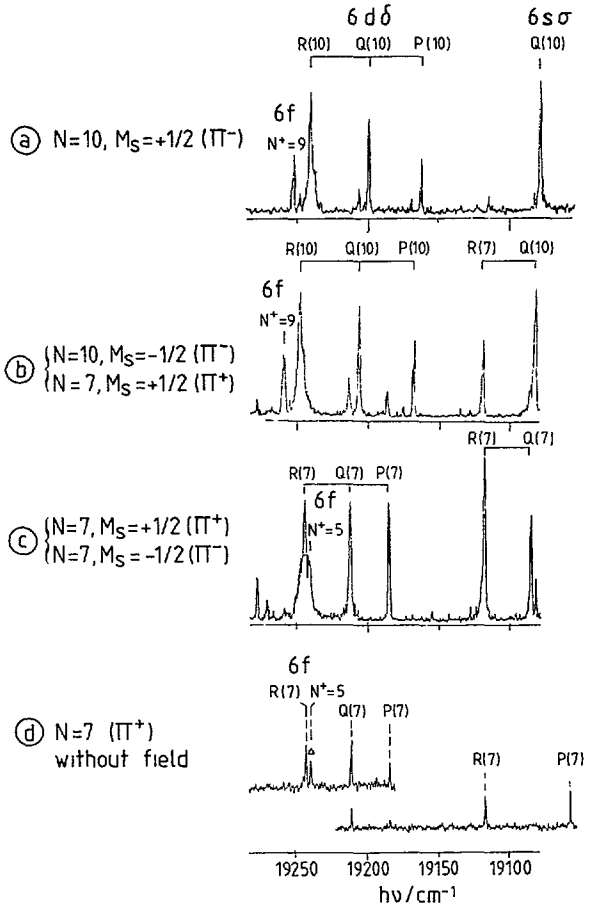

Fig. 5. — Portion of the two-color REMPI spectra from the intermediate C $^2\Pi$ ($v = 0$) state to the 6s, d ($v = 0$) supercomplex. Only transitions to the 6dδ and 6sσ are shown. The spectra (a), (b) and (c) have been recorded with a magnetic field of 0.93 T. The (d) spectrum, taken from reference [11], has been recorded without external field and is displayed for comparison with the (c) spectrum. (a) intermediate level $N = 10$, Π^-, $M_s = + 1/2$, pumped *via* the two-photon $Q_{21}(9\ 1/2)$ line of the C ← X transition. (b) intermediate levels $N = 10$, Π^-, $M_s = - 1/2$ and $N = 7$, Π^+, $M_s = + 1/2$, pumped *via* the overlapped two-photon lines $Q_{21}(9\ 1/2)$ and $S_{11}(5\ 1/2)$, respectively. (c) intermediate levels $N = 7$, Π^+, $M_s = + 1/2$ and $N = 7$, Π^-, $M_s = - 1/2$, pumped *via* the overlapped two-photon lines $S_{11}(5\ 1/2)$ and $R_{21}(5\ 1/2)$, respectively. (d) intermediate level $N = 7$, Π^+, pumped *via* the $N_{12}(9\ 1/2)$ three-photon line of the C ← X transition. Note the 6f, $N^+ = 9$ lines in (a) and (b) and the 6f, $N^+ = 5$ line in (c), arising from perturbation with the nearby 6d transitions and showing a broader Zeeman profile than the 6d lines. The probe laser bandwidth is of the order of 0.3 cm^{-1}

instance, the zero field spectrum of figure 7a corresponds to the diagram of figure 6. As shown by the P, Q, R splitting inside each rotational N^+ series, and from the splitting between the ℓ (or N) components in figure 3, the effective molecular anisotropy is of the order of a few cm^{-1}, i.e., larger than the LZE interaction (typically 0.5 cm^{-1}). On the other hand, it is about 10 times or more smaller than the splitting between different N levels (N and $N \pm 1$) in the 6s, d supercomplex. This means that the magnetic perturbation acts more efficiently in the 4f level than in the 6s, d levels. Indeed, deviations from the zero field

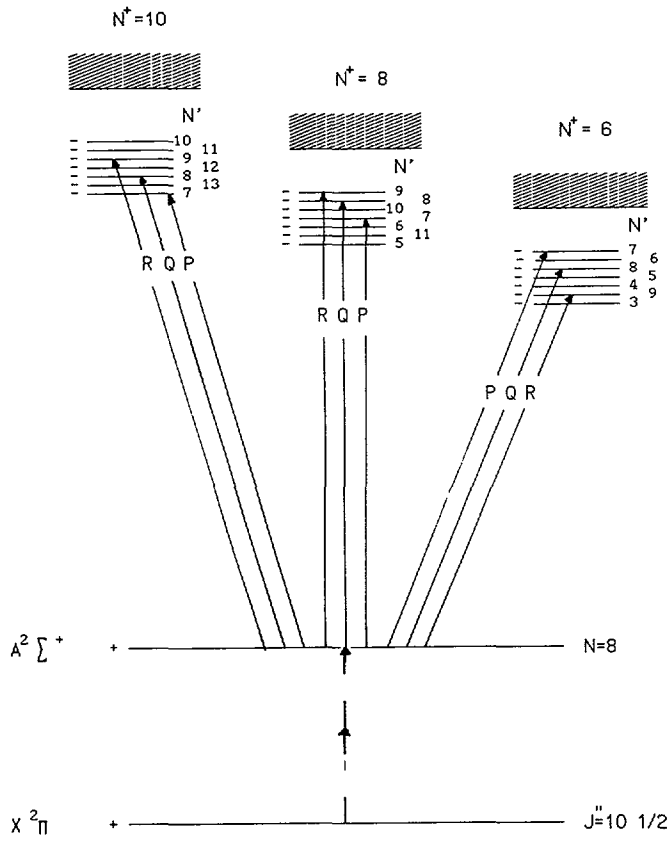

Fig. 6. — Transition diagram for the $nf(v = 1) \leftarrow A\ ^2\Sigma^+(v = 1)$ probe step of the two-color REMPI process. The intermediate rotational level $N = 8$ of the A state is pumped by a two-photon $O_{12}(10\ 1/2)$ line. The nf state is presented in a Hund's case (d) description. Only upper levels with negative total parity are shown in this diagram (transitions to positive total parity levels are forbidden). The unusual energy order of the various N' sublevels of the nf state for each N^+ comes from the long range anisotropic interaction as shown in figure 3. Nine rotational series are allowed, converging to $N^+ = 6$, 8 and 10.

pattern, both in intensity and in linewidth, are observed in figures 7b and 7d. Although the Zeeman splitting between the M_N components is not resolved in these spectra, the convoluted linewidths are in agreement with the calculated LZE in the « coupled Hund's case (d) » as it has been described in details in a previous paper [13]. N remains a good quantum number (P, Q and R lines are still defined) except when an accidental degeneracy occurs between two levels with N and $N \pm 1$. In a zero field situation, these N and $N \pm 1$ levels do not interact at any order and the corresponding lines simply overlap. When a magnetic field (even very small) is applied, these levels are completely mixed, N is no longer a good quantum number and a lift of degeneracy is observed. Such a situation occurs for the $N^+ = 3$, $\ell = 0$ and $N^+ = 3$, $\ell = +1$ levels as shown in the zero field diagram of figure 3b. Instead of the two overlapped $^0Q_0$ and $^0R_1$ lines of figure 7c, the Zeeman spectrum of figure 7d exhibit a doublet of mixed « Q + R » lines indicating a accidental decoupling of ℓ by the magnetic field.

When n increases, the effective molecular anisotropy rapidly decreases and becomes of the order of magnitude of the Zeeman perturbation or even smaller. As shown in the diagram of

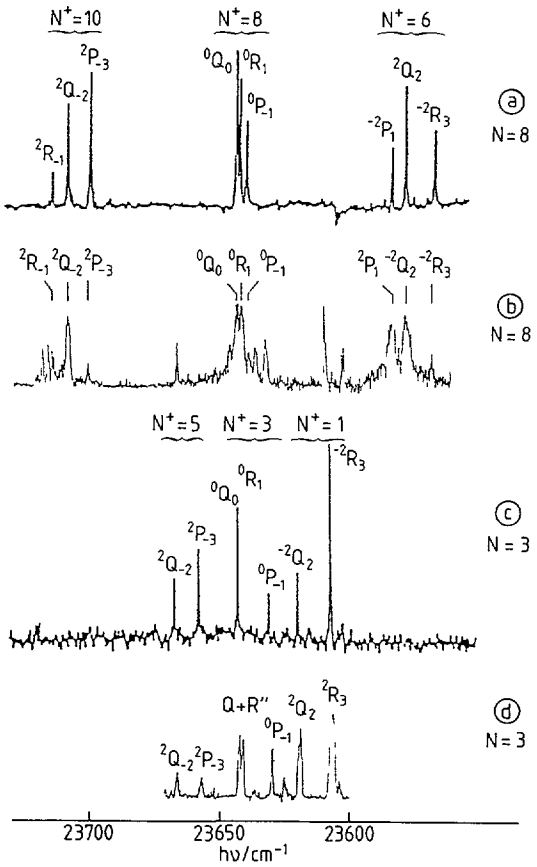

Fig. 7. — Spectrum of the 4f($v = 1$) ← A $^2\Sigma^+$ ($v = 1$) probe transition corresponding to the energy diagram of figure 5, without external field ((a) and (c)) and in a 0.93 T magnetic field ((b) and (d)). The spectra (a) and (c) are taken from reference [4] for comparison. (a) and (b) intermediate rotational level $N = 8$ in the A state, pumped *via* the two-photon O_{12}(10 1/2) line of the A ← X transition. (c) and (d) intermediate rotational level $N = 3$ in the A state, pumped *via* the two-photon O_{12}(5 1/2) line of the A ← X transition. Same laser bandwidth as in the spectra of figure 6. The lines are labelled $^{N^+ - N}\Delta N_{\ell}$ following the rule for case (b)-to-case (d) transitions [4].

figure 3a, the electronic splittings due to the long range interactions are of the order of 0.1 cm^{-1} in the 15f level, i.e., smaller than the LZE magnitude. When a 1 T magnetic field is applied, ℓ is no longer quantized along the rotational axis but rather along the field axis. N (or $\ell = N - N^+$) becomes a « mixed quantum number » while the projection of ℓ along the field axis, m_ℓ, becomes a good quantum number. ℓ and N^+ now precess independently around the magnetic field. This is the decoupled situation, or « decoupled Hund's case (d) », described in reference [13], in which the rotational-Zeeman levels are characterized by the quantum numbers (N^+, m_ℓ) instead of the « coupled Hund's case (d) » quantum numbers (N^+, N). Figure 8 shows part of the high resolution spectrum of the 15f levels probed from the intermediate levels $N = 3$, $M_s = -1/2$ and $N = 4$, $M_s = -1/2$ of the A state, respectively. The $N^+ = 2$ and $N^+ = 5$ levels of the 15f complex (Figs. 8a and 8b, respectively) as well as the $N^+ = 6$ level of the 14f complex exhibit a regular Zeeman pattern with five m_ℓ components, $m_\ell = -2, \ldots, +2$, as expected from the d character of the intermediate A

state and the $\Delta m_\ell = 0$ selection rule for the probe transition with the laser linearly polarized parallel to the magnetic field [13]. The M_{N^+} structure within each m_ℓ level is not resolved since it is proportional to the nuclear magneton (about 2 000 times smaller than the Bohr magneton).

The calculated spectra of figure 8 have been computed by setting a perturbation matrix diagonal in M_N and N^+ and including the Zeeman mixing between different N levels [13]. The good agreement between the calculated and the observed spectra indicates that channel mixing in the nf states is negligible. In this « strong field regime », the molecule behaves exactly like a Rydberg atom within each rotational channel N^+ with the molecular anisotropic structure completely hidden by the dominating magnetic interaction. These spectra bring an experimental evidence for a Paschen-Back effect in a molecule, as was firstly reported in [13].

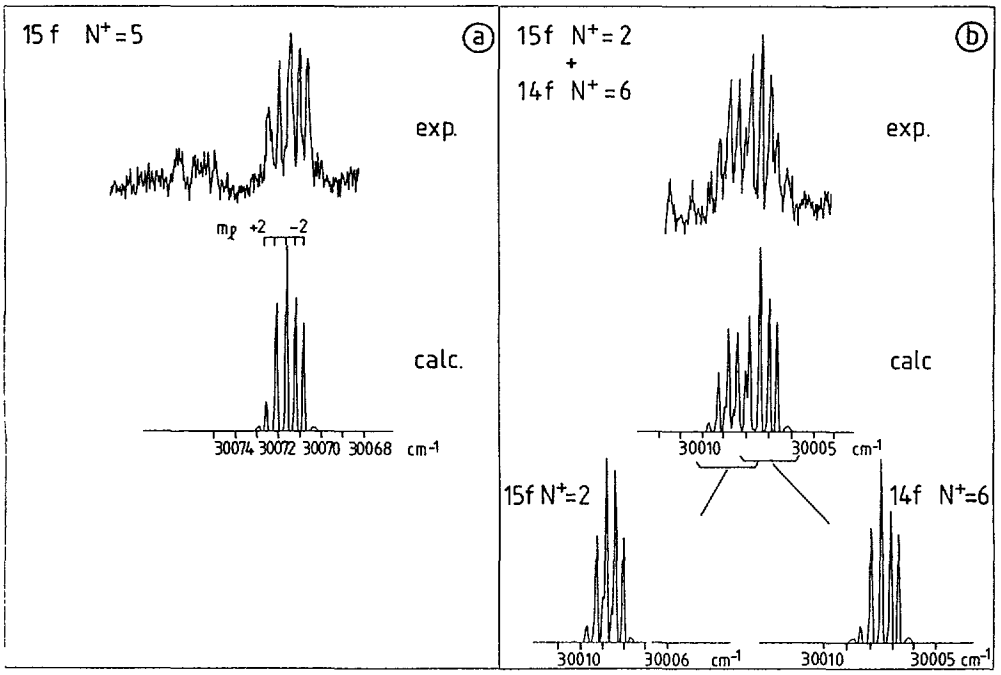

Fig. 8. — Observed and calculated Zeeman structure of the 15f level probed from different rotational levels of the A state (a) $N^+ = 5$ manifold probed from $N = 3$, $M_s = -1/2$; (b) $N^+ = 2$ manifold probed from $N = 4$, $M_s = -1/2$. The calculated spectra have been computed as in reference [13] (see the text). In (b), the lower member, $N^+ = 2$, of the 15f complex overlap the higher member $N^+ = 6$ of the 14f complex without interacting with it. The resulting convoluted spectrum corresponds to the sum of the two calculated spectra shown in the bottom and is in very good agreement with the experimental spectrum.

4.2 THE PENETRATING np SERIES : MQDT CALCULATIONS OF THE LINEAR ZEEMAN EFFECT. — Unlike the nonpenetrating nf states, the np series of NO have large quantum defects (of about 0.7) [2] giving rise to an important molecular anisotropy. The effective molecular anisotropy remains strong for a large range of n so that the np states are less sensitive to an external magnetic field perturbation than the nf states are. A theoretical approach well adapted for these states is given by the multichannel quantum defect theory (MQDT) which

takes into account the rotational channel mixing. The details of the MQDT treatment of the linear Zeeman effect have been given elsewhere [20].

Briefly, the anisotropy created by the magnetic field in the space-fixed reference frame leads to a mixing of states with different N values. Only the projection M_N of N along the field axis remains a good quantum number. In addition, at very large electron-core separation, the linear Zeeman interaction is dominating as compared with the rovibronic and Coulomb interactions. As a consequence, the projection m_ℓ of ℓ along the field axis becomes a good quantum number. In the MQDT framework, three different regions have to be considered in order to account for the different quantization axis for the Rydberg electron angular momentum ℓ. At short range, where the molecular anisotropy dominates, ℓ is quantized along the internuclear axis (Hund's case (b) description). At long range, where the rotational coupling dominates, ℓ is quantized along the N axis of the rotating core (coupled Hund's case (d) description). At very long range, where the field perturbation dominates, ℓ is quantized along the field axis (uncoupled Hund's case (d) description). This third range was introduced by Monteiro and Taylor [21] in their treatment of the linear Zeeman effect in the MDQT approach. They introduced new asymptotic ionization channels « dressed » by the magnetic field and defined by the set of quantum numbers (N^+, ℓ, m_ℓ) and by the ionization energy $E_{N^+} + \mu_B B m_\ell$, where E_{N^+} is the zero-field ionization energy in channel N^+ and $\mu_B B m_\ell$ is the Paschen-Back energy of the ionic core. In addition, they introduced two frame transformations instead of one as in the zero-field MQDT treatment. The first frame transformation connects the « isotropic » space-fixed (coupled Hund's case (d)) and the body-fixed (Hund's case (b)) total wave functions. The second frame transformation connects the « field oriented » space-fixed (uncoupled Hund's case (d)) with the « isotropic » space-fixed (coupled Hund's case (d)) total wavefunctions.

If an unrealistic isotropic situation for the molecular field is assumed, the MQDT predicts that all the M_N sublevels associated with a given ℓ, m_ℓ level are strictly degenerate in energy, leading to an atomic structure within each N^+ rotational channel. In a real molecule, this extreme situation is approached, although never completely achieved, either for nonpenetrating states (as the 15f state discussed above) or for very high n Rydberg levels, i.e., in all cases for a very weak effective molecular anisotropy. In this case, the magnetic field imposes its anisotropy and an m_ℓ atomic structure occurs in which the molecular M_N substructure has completely collapsed. On the contrary, for the low np Rydberg states, m_ℓ is not yet a good quantum number because the m_ℓ levels are mixed by the strong molecular anisotropy. N is still a good quantum number and a molecular Zeeman M_N structure occurs.

The np series of NO between $n = 8$ and $n = 22$ illustrate the intermediate situations occurring between the two extreme situations described above, as shown by their calculated spectra in a 1 T and a 5 T field of figures 9 and 10, respectively. In these figures, the calculated oscillator strengths have been normalized (multiplied by n^{*3} in which n^* is the effective principal quantum number) in order to better compare the different np spectra. Note that this effective oscillator strength surprisingly seems to increase with n^*. This effect comes only from the gradual collapse of three lines or groups of lines into almost one line for high n^* values. In both figures, the transitions have been calculated from the intermediate $N = 3$, $M_s = -1/2$, level of the A $^2\Sigma^+$, $v = 1$ state. All the calculated transitions have been convoluted with a width of 0.07 cm^{-1}.

Five np series are allowed from the A state, i.e., three series (P, Q and R) converging to $N^+ = 3$, one R series converging to $N^+ = 5$ and one P series converging to $N^+ = 1$. MQDT predicts that the strongest series are the ones converging to $N^+ = 3$, the other ones being allowed *via* channel mixing only. The intensity of the $N^+ = 1$ and $N^+ = 5$ series rapidly decreases as the effective molecular anisotropy decreases. Consequently, only the transitions

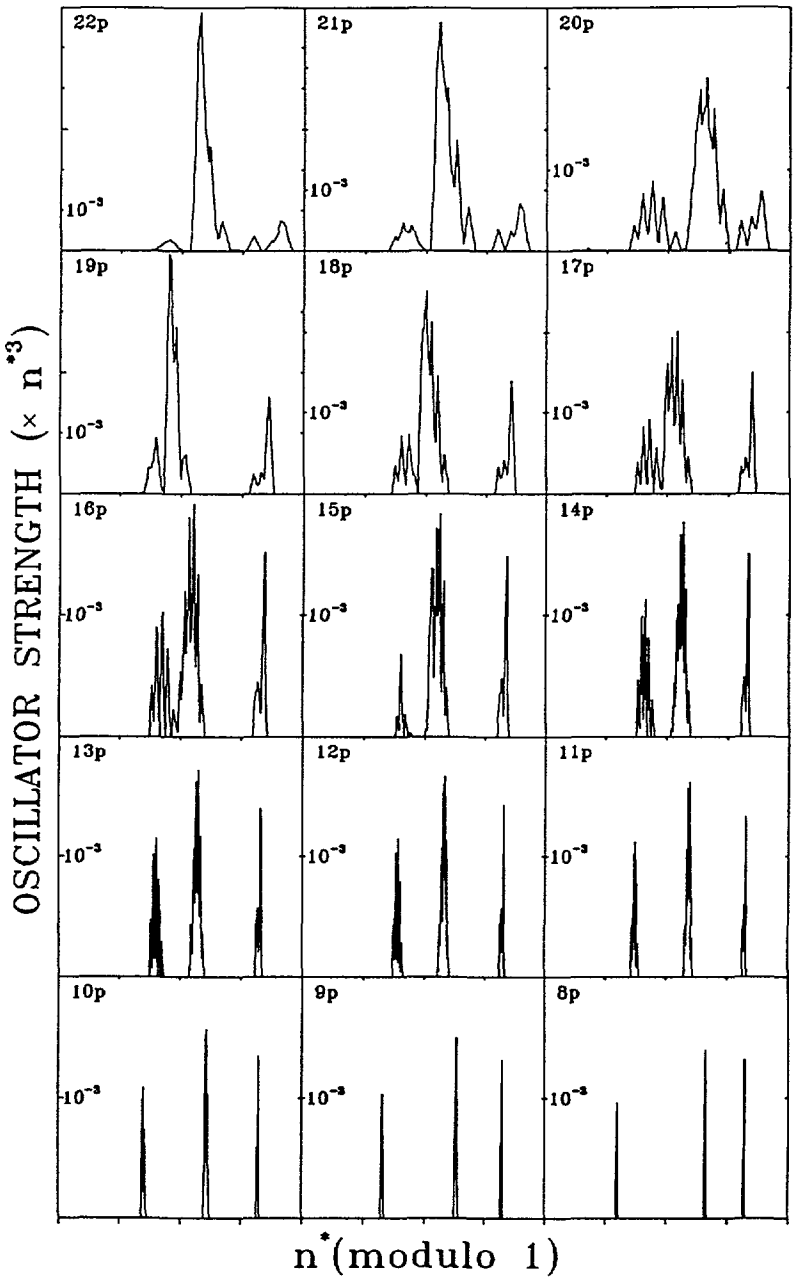

Fig. 9. — MQDT calculated spectrum of the np series between $n = 8$ and $n = 22$, from the intermediate level A $^2\Sigma^+$, $N = 3$, $M_s = -1/2$, in a 1 T field. The horizontal scale corresponds to the effective principal quantum number $n^* = n - \mu$ modulo 1. Successive divisions correspond to increments of 0.025. For instance, for the 8p spectrum the bottom scale varies from 7.25 to 7.35 from the right to the left and corresponds to a total energy variation between 75 001.8 cm^{-1} to 75 058.2 cm^{-1} On the other hand, the energy spread is much lower in the 22p level, of about 2 cm^{-1} instead of 56 cm^{-1} The vertical scale gives the normalized oscillator strengths. Successive divisions correspond to increments of 10^{-3}

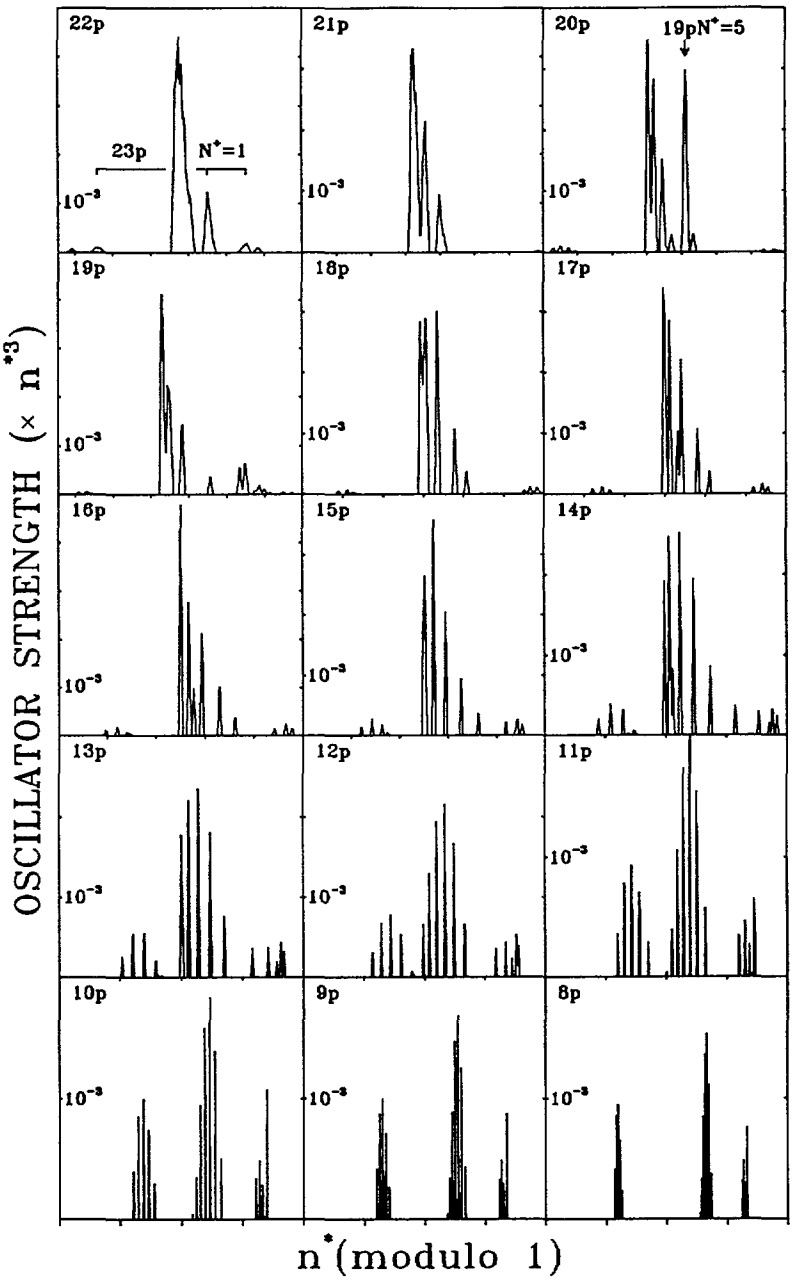

Fig. 10. — MQDT calculated spectrum of the np series between $n = 8$ and $n = 22$, from the intermediate level A $^2\Sigma^+$, $N = 3$, $M_s = -1/2$, in a 5 T field. Same scale as in figure 9.

to the $N^+ = 3$ levels are presented in figures 9 and 10, since they carry most of the total oscillator strength for the np series.

For the lowest 8p state shown in the bottom of figure 9, a Born Oppenheimer (Hund's case (b)) situation occurs with three separated lines Q(Π^-), R(Π^+) and P(Σ^+) at 75 011.8 cm^{-1}, 75 021.4 cm^{-1} and 75 041.5 cm^{-1}, respectively (from the right to the left). The Zeeman effect

is negligibly small compared to the molecular anisotropy. With increasing n, as the effective anisotropy decreases, the three lines come closer one to the other. At the same time, the energy scale decreases as $1/n^{*3}$ in such a way that the constant Zeeman interaction becomes significant by comparison with the molecular anisotropy. The M_N structure is more and more spread due to the expansion of the energy scale (the energy range is 56.4 cm^{-1} on the 8p spectrum while it is only 2 cm^{-1} on the 22p spectrum). Nevertheless, when the spacing between the different N lines become comparable to the Zeeman perturbation this structure starts to collapse and is gradually replaced by a m_ℓ structure. In the highest level of this figure, the 22p level, the m_ℓ structure clearly shows up with a strong $m_\ell = 0$ line, as expected from the 3s orbital of the A state and two weak $m_\ell = \pm 1$ lines which are the manifestation of a residual m_ℓ mixing by the molecular anisotropy. Intensity anomalies appears in some spectra as in the 15p and in the 20p spectra. They originate from local channel interaction. For instance, the higher energy peak in the 15p manifold looses intensity by interaction with the 14p, $N^+ = 7$ level and the overall intensity of the 20p level is decreased by interaction with the 19p, $N^+ = 5$ level.

In the 5 T spectra of figure 10, the Zeeman structure is spread by a factor of 5 with respect to the spectra of figure 10. Up to the 11p level, the 7 M_N components expected for the R and Q lines and the 5 M_N components expected for the P line, from the $N = 3$ level of the A state are well resolved. For higher n^*, they start to overlap and gradually collapse into m_ℓ components. In the 15p spectrum, the m_ℓ structure is already apparent with a strong $m_\ell = 0$ manifold of partially overlapped M_N components and two weak $m_\ell = +1$ and $m_\ell = -1$ manifolds. Finally, the 22p state in a 5 T field exhibits an almost perfect atomic structure with a single $m_\ell = 0$ line in which all the M_N components are quasi degenerate (very weak $m_\ell = +1$ and $m_\ell = -1$ appear nevertheless because of interaction with the 23p, $N^+ = 1$ level). As in the 1 T spectra, local perturbations occur as in the 20p level.

5. Conclusion.

The external magnetic field applied to a Rydberg molecule has been shown to play the role of a sensitive probe for the molecular coupling between the Rydberg electron and the molecular core. Successive frame transformations are necessary to describe the motion of this electron from the core region to the outer field region. Contrary to a Rydberg atom in a magnetic field, for which only the anisotropy of the field competes with the spherical Coulomb attraction, a Rydberg molecule exhibits a larger variety of situations due to the presence of the molecular core anisotropy and to the competition between this anisotropy and the field anisotropy. At very large distances from the core, and consequently for very high n levels, the field perturbation takes over all the other interactions and the Rydberg molecule exhibit an atomic like structure within each rotational channel. Such an extreme situation occurs when the electron is decoupled enough from the molecular frame and when its motion is well described in the space-fixed frame (Hund's case (d)). If such a condition is not well fulfilled, extremely high fields are necessary to decouple the electron from the molecular frame. Indeed, as shown in figure 10, a strong field of 5 T does not significantly change the molecular structure of the low and intermediate np levels.

At the same time, the rotational structure of the molecular core is, in all cases, little affected by the magnetic perturbation. Once again, a complete shake up of the molecular structure by the magnetic field, involving the rotational structure, needs the presence of strong channel mixing. This N^+ channel mixing originates from the molecular anisotropy only, while the N mixing originates from the field anisotropy. This means that both kinds of anisotropy are required simultaneously in order to strongly perturb the structure of a Rydberg molecule.

As in Rydberg atoms, a strong field regime occurs when the quadratic Zeeman effect starts to dominate the magnetic interaction of equation (1). Such a situation has been observed in the high np series of NO, even in a moderately strong field of 1 T [22]. Then ℓ mixing also occurs leading to a spread of the oscillator strength over a large number of close lying transitions. The new aspect presented by such a molecular situation is that the different rotational channels exhibit smaller energy gaps between each other as compared with an atomic situation giving rise to a new domain of investigations.

References

[1] JUNGEN Ch. and MIESCHER E., *Can. J. Phys.* **47** (1969) 1769.

[2] MIESCHER E. and HUBER K. P., International Revue of Science (*Phys. Chem.* Ser. 2) **3** A. D. Buckingham and D. A. Ramsay Eds. (Butterworths, 1976) p. 37.

[3] CHEUNG W. Y. and COLSON S. T., Advances in Laser Spectroscopy, **2** B. A. Garetz and J. R. Lombardi Eds. (Wiley, 1983) p. 73.

[4] CHEUNG W. Y., CHUPKA W. A., COLSON S. D., GAUYACQ D., AVOURIS Ph. and WYNNE J. J., *J. Chem. Phys.* **78** (1983) 3625.

[5] SEAVER M., CHUPKA W. A., COLSON S. D. and GAUYACQ D., *J. Phys. Chem.* **87** (1983) 2226.

[6] EBATA T., ANEZAKI Y., FUJII M., MIKAMI N. and ITO M., *Chem. Phys.* **84** (1984) 151.

[7] ANEZAKI Y., EBATA T., MIKAMI N. and ITO M., *Chem. Phys.* **89** (1984) 103 ; **97** (1985) 153.

[8] VERSCHUUR J. W. J., KIMMAN J., VAN LINDEN VAN DEN HEUVEL H. B. and VAN DER WIEL M. J., *Chem. Phys.* **103** (1986) 359.

[9] CHEUNG W. Y., CHUPKA W. A., COLSON S. D., GAUYACQ D., AVOURIS Ph. and WYNNE J. J., *J. Phys. Chem.* **90** (1986) 1086.

[10] BIERNACKI D. T., COLSON S. D. and EYLER E. E., *J. Chem. Phys.* **88** (1988) 2099.

[11] FREDIN S., GAUYACQ D., HORANI M., JUNGEN Ch., LEFEVRE G. and MASNOU-SEEUWS F., *Mol. Phys.* **60** (1987) 825.

[12] GAUYACQ D., ROCHE A. L., SEAVER M., COLSON S. D. and CHUPKA W. A., *Mol. Phys.* **71** (1990) 1311.

[13] GUIZARD S., SHAFIZADEH N., HORANI M. and GAUYACQ D., *J. Chem. Phys.* **94** (1991) 7046.

[14] KRUIT P. and READ F. H., *J. Phys. E* **16** (1983) 313.

[15] MIESCHER E., *Can J. Phys.* **54** (1976) 2074.

[16] JUNGEN Ch., *J. Chem. Phys.* **53** (1970) 4168.

[17] EYLER E. E. and PIPKIN F., *Phys. Rev. A* **27** (1983) 2462.

[18] HERZBERG G., Molecular Spectra and Molecular Structure I. Spectra of Diatomic Molecules (Van Nostrand Reinhold, Princeton, 1950) pp. 300-306.

[19] GUIZARD S., SHAFIZADEH N., CHAPOULARD D., HORANI M. and GAUYACQ D., *Chem. Phys.* **156** (1991) 509.

[20] RAOULT M., GUIZARD S. and GAUYACQ D., *J. Chem. Phys.* **95** (1991) 8853.

[21] MONTEIRO T. S. and TAYLOR K. T., *J. Phys. B : At. Mol. Phys.* **22** (1989) L191.

[22] GUIZARD S., SHAFIZADEH N., RAOULT M. and GAUYACQ D., to be published.